DOI: 10.1002/cssc.201402651

Comparative Studies on Rigid π Linker-Based Organic Dyes: Structure–Property Relationships and Photovoltaic Performance

Hairong Li,[a] Teck Ming Koh,[a] Yan Hao,[a, b] Feng Zhou,[a] Yuichiro Abe,[a] Haibin Su,[a] Anders Hagfeldt,[b] and Andrew C. Grimsdale*[a]

A series of six structurally correlated donor–π bridge–acceptor organic dyes were designed, synthesized, and applied as sensitizers in dye-sensitized solar cells. Using the most widely studied donor (triarylamine) and cyclopenta[1,2-b:5,4-b′]dithiophene or cyclopenta[1,2-b:5,4-b′]dithiophene[2′,1′:4,5]thieno[2,3-d]thiophene as π spacers, their structure–property relationships were investigated in depth by photophysical techniques and theoretical calculations. It was found that the photovoltaic performance of these dyes largely depends on their electronic structures, which requires synergistic interaction between donors and acceptors. Increasing the electron richness of the donor or the elongation of π-conjugated bridges does not necessarily lead to higher performance. Rather, it is essential to rationally design the dyes by balancing their light-harvesting capability with achieving suitable energy levels to guarantee unimpeded charge separation and transport.

Introduction

In the classical configuration of dye-sensitized solar cells (DSCs) first proposed by Grätzel et al. in 1991,[1] the sensitizer is one of the most important components in the device because it is responsible for light harvesting. Despite the large number of reports on DSCs over the decades exploring efficient, robust, cost-effective, and eco-friendly architectures, the development of sensitizers still remains a major research activity. Therefore, a variety of sensitizers has been developed, including metal–organic complexes,[2] organic dyes,[2a,3] inorganic quantum dots,[4] and, recently, perovskites.[5] The first generation of sensitizers (metal complexes, including metal–pyridyl complexes, porphyrins, and phthalocyanines) has shown excellent performance and still undergoes optimization of their properties and device efficiencies; a power-conversion efficiency (PCE) of 13.0% is the best achieved to date.[6,7] However, they often suffer from problems, such as high toxicity, high cost (low synthetic yield and use of rare metals), and compatibility in all-solid-state devices. On the other hand, organic sensitizers possess the advantages of structural diversity, which enables fine-tuning of their properties, lower cost of production and, importantly, high extinction coefficients.

Among the various types of organic sensitizers, optimizing the donor–π bridge–acceptor geometry is particularly important for obtaining efficient intramolecular charge transfer from a donor, such as arylamine, through a π bridge to an acceptor (predominantly cyanoacetic acid) anchored to a mesoporous TiO_2 surface to facilitate charge separation and injection. In this scenario, the π component usually plays two major roles: first, it largely determines the electronic properties of the sensitizer, such as the HOMO energy level, which is related to dye-regeneration efficiency, the LUMO energy, which affects charge injection, and the absorption window and coefficient, which determine light-harvesting capability; second, it physically separates the donor from the TiO_2 surface to impede charge recombination between injected electrons and the oxidized sensitizer.[8] However, there exists the possibility for nonradiative decay of the excited sensitizer due to molecular vibration.[9] As a result, it is critical to make the molecule rigid to reduce nonradiative decay, but this in turn may induce strong aggregation, which decreases electron injection. Cyclopenta[1,2-b:5,4-b′]dithiophene (CPDT)-based organic dyes such as Y123,[10] C218,[11] and JF419,[12] which possess a rigid and extended π core, aggregation is suppressed using appropriate alkyl groups on sp^3 bridgehead carbon atoms; in this way, the above contradiction is successfully solved and a high PCE value of 10.3% is achieved in a cobalt electrolyte-based liquid DSC.[12] Meanwhile, cyclopenta[1,2-b:5,4-b′]dithiophene[2′,1′:4,5]thieno[2,3-d]thiophene (CPDTTT), which is a similar building block with more π planarity, was initially developed as a donor unit in conjugated polymers for organic photovoltaics (OPV),[13] and was later used as a π linker in an organic dye (C243).[14] Because CPDTTT

---

[a] Dr. H. Li, T. M. Koh, Dr. Y. Hao, Dr. F. Zhou, Y. Abe, Prof. H. Su, Prof. A. C. Grimsdale
Energy Research Institute @ NTU (ERI@N)
School of Materials Science and Engineering
Nanyang Technological University
Nanyang Avenue, Singapore 637553 (Singapore)
E-mail: acgrimsdale@ntu.edu.sg

[b] Dr. Y. Hao, Prof. A. Hagfeldt
Department of Chemistry
Ångström Laboratory
Uppsala University
Box 523, 75120 Uppsala (Sweden)

Supporting Information for this article is available on the WWW under http://dx.doi.org/10.1002/cssc.201402651.

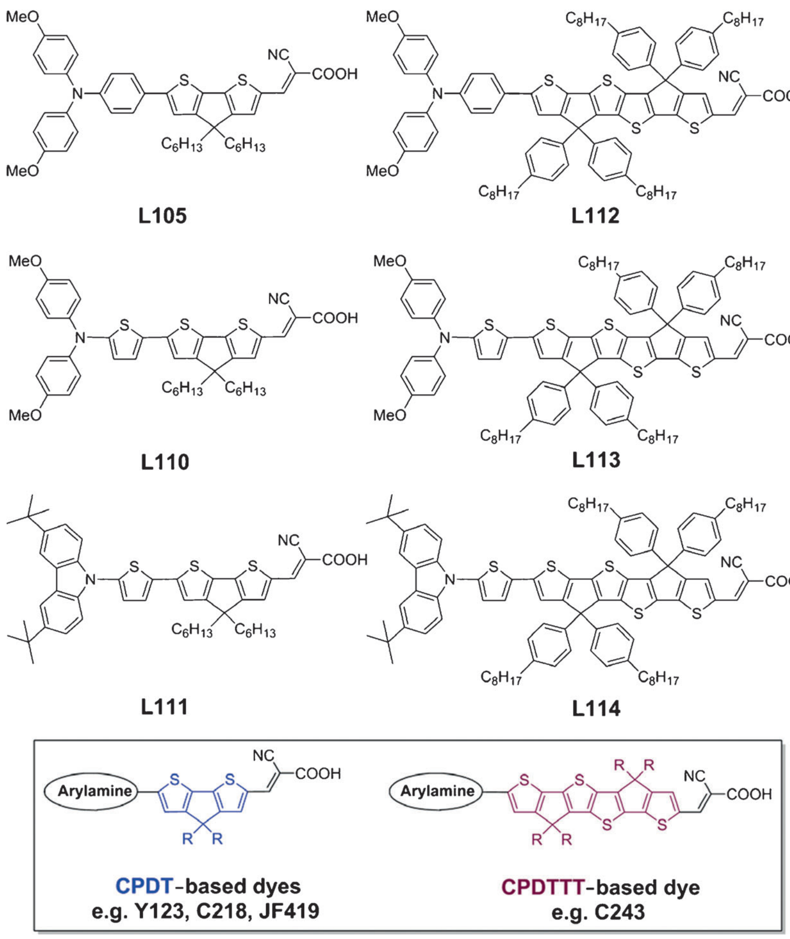

Figure 1. Chemical structures of the six organic dyes with permutation of three different donors and two different spacers (CPDT and CPDTTT).

can be viewed as the π extension of a CPDT unit and both have rigid and planar structures, we were interested in understanding their structure–property relationships. We herein report six structurally correlated donor–π bridge–acceptor dyes (Figure 1), which can be categorized into two groups, with CPDT and CPDTTT as the π linker for each group. Among each group, three different donors of different electron-donating strength were adopted with the acceptor remaining the same. Detailed studies including theoretical calculations, device performance, as well as electrochemical and photophysical measurements were carried out to understand how the interplay of donor and π linker structures affects their photophysical properties and device performance.

Results and Discussion

Characterization

Synthetic routes are summarized in Scheme 1. The six donor–π bridge–acceptor dyes (Figure 1) can be divided into two groups for ease of discussion: group A (**L105**, **L110**, **L111**) and group B (**L112**, **L113**, **L114**). Groups A and B have, respectively, CPDT and CPDTTT as π linkers. Each group contains three different donors: *N*,*N*′-bis(4-methoxyphenyl)-*N*-phenylamine (**L105**, **L112**), *N*,*N*′-bis(4-methoxyphenyl)-*N*-thiophene-2-amine (**L110**, **L113**), and 3,6-di-*tert*-butyl-9-(thiophen-2-yl)-9*H*-carbazole (**L111**, **L114**) with the shortest possible alkyl chains to minimize the physically blocking effect on charge recombination so that the intrinsic electronic properties of dyes become manifest. Both absorption (Figure 2) and cyclic voltammetry (CV) measurements of the six dyes were recorded in dichloromethane (see the Supporting Information, Figure S1); HOMO, LUMO, optical bandgap (E_g), absorption peak maximum (λ_{max}), and the corresponding molar absorption coefficient (ε) values are summarized in Table 1. Within each group, bandgap values increase in the order of **L110** < **L105** < **L111** in group A and **L113** < **L112** < **L114** in group B, which indicates that the donor part of **L110** and **L113**, that is *N*,*N*′-bis(4-methoxyphenyl)-*N*-thiophene-2-amine, has the strongest electron-donating capability among the three, producing bandgaps of 1.80 and 1.77 eV, respectively. It is also easy to deduce from group A that 3,6-di-*tert*-butyl-9-(thiophen-2-yl)-9*H*-carbazole has a significantly weaker electron-donating effect relative to the other two donors because **L111** has a bandgap value of 2.04 eV, whereas **L112** with a moderate donor shows a bandgap value of 1.89 eV. A similar trend is also observed in absorption peak maximum values: the λ_{max} value of **L111** is 519 nm and that of **L105** is 553 nm. Though **L105** and **L110** have almost equal

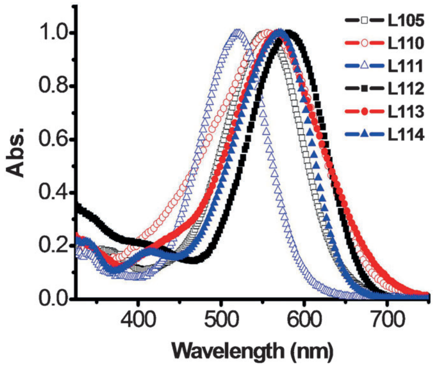

Figure 2. Absorption spectra of the six dyes in dichloromethane (DCM).

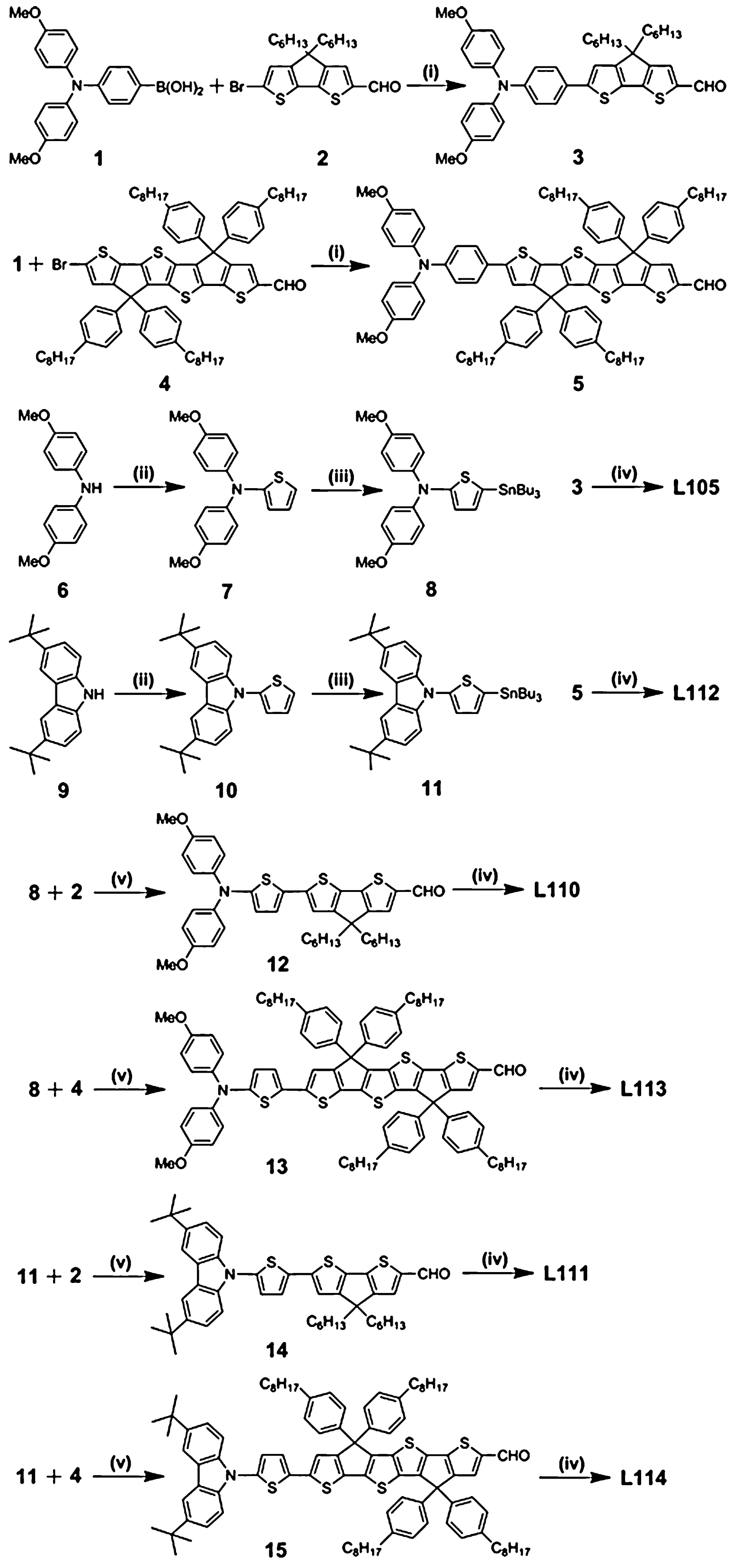

Scheme 1. Synthetic routes to the six dyes. Reaction conditions: (i) K_2CO_3, [Pd(PPh$_3$)$_4$], THF/H$_2$O, reflux; (ii) 2-bromothiophene, [Pd(dba)$_2$] (dba = dibenzylidenacetone), *t*BuOK, P(*t*Bu)$_3$·HBF$_4$, toluene, 95 °C; (iii) *n*BuLi, SnBu$_3$Cl, THF, −78 °C to RT; (iv) CNCH$_2$COOH, piperidine, CHCl$_3$, reflux; (v) [PdCl$_2$(PPh$_3$)$_2$], THF, reflux.

values of λ_{max} (556 and 553 nm, respectively), **L110** has clearly a more red-shifted absorption onset, and therefore a lower bandgap. All the dyes in group B show red-shifted absorptions relative to their corresponding analogues in group A, indicating that stronger electron delocalization takes place in the CPDTTT linker. Within group B the general trend remains the same, but the differences in both bandgap and absorption peak maximum become less obvious. But it is worth noting that the λ_{max} value of **L114** is 571 nm, which is drastically red-shifted by 52 nm from that of **L111**, as a result of the extended conjugation superseding the weak donor.

From CV studies (Table 1; also see the Supporting Information, Figure S1), all the dyes have different HOMO values. Interestingly, **L105** and **L112** had similar LUMO values, and that also applies for the pairs of **L110**/**L113** and **L111**/**L114**. This indicates that the extended linker affects the HOMO more than the LUMO probably due to its electron-rich nature. Because the acceptor part was designed to be the same, that also explains why the absorption spectra become similar among dyes in group B. All these results strongly imply that CPDTTT does not only act as a strong electron-delocalizing π linker, but also becomes a part of the donor part in group B dyes. Certainly, the donors still played their roles, but were weakened; otherwise we would observe the same HOMO levels in group B. It is worth mentioning that the difference between **L110** and **L113** is least obvious in terms of bandgap (1.80 versus 1.77 eV, respectively) and λ_{max} (556 vs. 569 nm, respectively) relative to the other two pairs (i.e., **L105**/**L112** and **L111**/**L114**), manifesting the dominant effect of the donor determining the HOMO levels of **L110** and **L113**,

Table 1. Output of UV/Vis and electrochemical characterization of the dyes.

Dye	HOMO [eV]	LUMO [eV]	E_g [eV]	λ_{max} [nm]	ε [10^4 L mol^{-1} cm^{-1}]
L105	−5.08	−3.19	1.89	553	6.15
L110	−4.91	−3.11	1.80	556	6.34
L111	−5.25	−3.21	2.04	519	4.09
L112	−5.01	−3.18	1.83	582	6.92
L113	−4.88	−3.11	1.77	569	6.77
L114	−5.13	−3.24	1.89	571	4.80

regardless of the strong electron-donating effect of the CPDTTT spacer.

DFT calculations

To gain insight into the electronic structures of the frontier orbitals of the six dye molecules, DFT calculations were performed on the B3LYP/6-31G* level. Their optimized ground-state molecular structures are presented in Figure 3.

As expected, all dye molecules possessed well separated HOMO and LUMO levels with partial overlap at the CPDT spacer, suggesting an efficient electron transition from the HOMO to the LUMO and then to the conduction band of TiO_2 through the anchor group. The LUMO has the highest electron density on the cyanoacetic acid unit amongst all dyes, whereas the situation in the HOMO varied. Among group A dyes, the HOMO of **L105** and **L110** is mainly delocalized over the arylamine unit and partially on the π spacer, whereas the electron density in **L111** is mainly found on the nitrogen-linked thiophene and the π spacer, which directly reflects the weak donor nature of the carbazole. Therefore, charge delocalization of **L111** was limited and resulted in higher bandgap values relative to the rest of the dye molecules (Table 1). In group B molecules, due to the more electron-rich CPDTT spacer, the HOMO level of both **L112** and **L113** shifted from arylamine to CPDTTT leading to less HOMO–LUMO separation. This undesirable situation, fortunately, was compensated by the effect of the larger and more electron-delocalized CPDTTT unit. As a result, both **L112** and **L113** still exhibited lower bandgap values relative to **L105** and **L110**, respectively. As for **L114**, the limitation of the weak carbazole donor was more conspicuous because there was no electron density in the HOMO on the carbazole unit (except on the nitrogen atom) and the CPDTTT spacer practically acted as the donor, just like **L111**. Nevertheless, due to CPDTTT being more electron-rich and electron-delocalized than CPDT, **L114** had a lower bandgap relative to **L111** as confirmed by absorption measurements. Our computational results confirmed the observations from absorption measurements: the larger red shift of λ_{max} from **L111** to **L114** (52 nm) relative to that from **L105** to **L112** (29 nm) or from **L110** to **L113** (13 nm) strongly indicated the interdependent relationship between spacer and donor (Table 1), that is the strong donor (**L113** and **L110**) suppressed the electron-donating effect of the spacer, whereas the weak donor enhanced that effect (**L114** and **L111**).

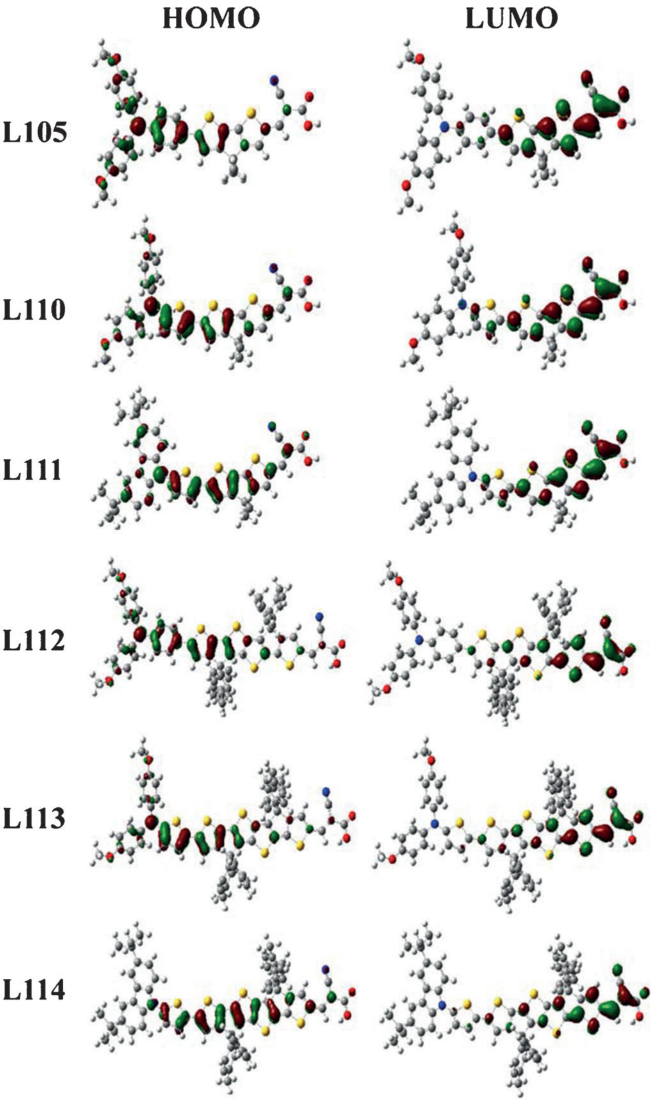

Figure 3. Molecular orbitals of the six dye molecules using the B3LYP functional and 6-31G* basis set under geometry optimization condition.

Photovoltaic performance

The action spectra of incident photon-to-current conversion efficiency (IPCE) for DSCs based on the six dyes are shown in Figure 4 and the corresponding absorbed photon-to-electron conversion efficiency (APCE), which takes into account light-harvesting efficiency is given in the Supporting Information (Figure S2). **L105** has a high IPCE plateau of 80 % from 450–600 nm, whereas **L112** has a relatively narrower IPCE plateau of 80 % from 500 to 600 nm. However, **L112** (with a CPDTTT spacer) has a lower bandgap and thus a broader absorption area (up to 750 nm) than **L105** (up to 700 nm), leading to the overall IPCE of **L112** over the whole absorption region being still a bit higher than that of **L105** (see J_{sc} in Table 2). On the other hand, **L110** and **L113**, which have broader absorption regions than the other four dyes, have poor IPCE performance, with a high plateau value of <60 % for both. This is probably due to the poor charge-regeneration process (as discussed earlier) because both of them have much higher HOMO levels

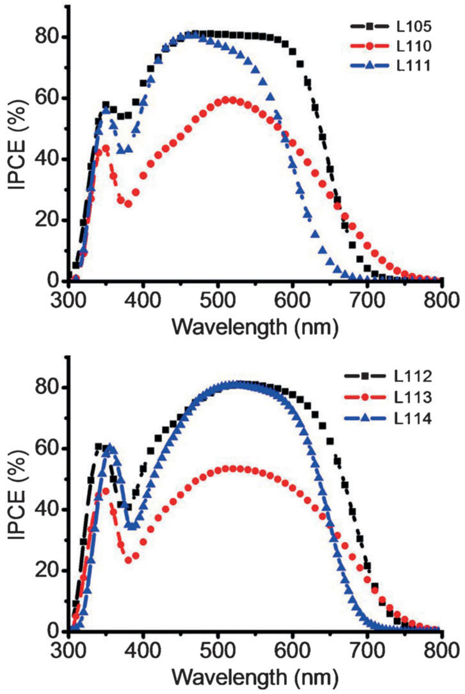

Figure 4. IPCE spectra of DSCs sensitized with the six dyes.

Table 2. Current–voltage characteristics of DSCs sensitized with the six dyes.

Dye	J_{sc} [mA cm^{-2}]	V_{oc} [V]	FF	PCE [%]
L105	14.6	0.73	0.69	7.32
L110	9.63	0.63	0.71	4.31
L111	10.5	0.68	0.73	5.19
L112	15.5	0.72	0.72	8.09
L113	9.88	0.64	0.71	4.45
L114	12.8	0.67	0.74	6.46

(Table 1) resulting in a reduced driving force for electron replenishment from redox couples. We ruled out the self-quenching effect because efficiency was not improved by adding chenodeoxycholic acid (CDCA) as co-absorber, which is not surprising because the π spacer has a sufficient number of bridged alkyl chains to suppress aggregation. **L111** has the largest bandgap and thus the narrowest absorption region. Therefore, though not as effective as **L105**, **L111** showed a decent photon-to-current response up to 650 nm and was overall better than **L110**. It is clear in Table 1 that **L114** (with a CPDTTT spacer) had a largest red shift (0.15 eV) in absorption relative to **L111** (with a CPDT spacer) among the three pairs of dyes (red shift of 0.06 eV from **L105** to **L112**; red shift of 0.03 eV from **L110** to **L113**). The direct consequence was the dramatic improvement in IPCE performance with an absorption of up to 700 nm, which was though still not comparable with **L105** and **L112**. The weaker donor capability of carbazole relative to triphenylamine is the limiting factor in light absorption for **L111**, which was improved by extended conjugation in **L114**.

The photovoltaic performance of DSCs sensitized by the six dyes was investigated under standard AM 1.5G irradiation (Figure 5 and Table 2). **L112** had the highest PCE of 8.1% among all six dyes and 10% higher than that of **L105**, which is mainly attributed to the higher short-circuit current (J_{sc}) of the former. The higher J_{sc}, as discussed earlier, is the result of the broad absorption and the high IPCE plateau region of 80%. By carefully examining device performance, we found that the open-circuit voltage (V_{oc}) of **L105** is always a little higher than that of **L112**, although the difference is small, which indicated that the recombination rate was somewhat higher in **L112**. Both **L110** and **L113** had disappointing photovoltaic performance, contrary to our initial expectations; J_{sc} and V_{oc} values were significantly lower than those of the other four dyes. Interestingly, both of them have similar values in every parameter (Table 2) including bandgap, as discussed earlier. Therefore, the origin of poor performance can only be attributed to the donor part. It may be argued that the strong donor does not necessarily improve photovoltaic performance because the more electron-rich donor raises the HOMO level causing the regeneration problem and the recombination rate could also increase concurrently. Whereas **L111** showed decent photovoltaic performance limited by its narrow absorption window, **L114** produced a PCE of 6.5%, which was 25% higher than that of **L111** (5.2%); V_{oc} and fill factor (FF) values for both dyes were comparable and the only major difference was J_{sc}, which thus determined the IPCE results. We conclude that in the case of dyes with a suitable donor (**L105** and **L112**), the main role of the π spacer is to modulate absorption; in the case of a strong but unsuitable donor (**L110** and **L113**), the electron-rich spacer is not able to play any role, which also indicates that incorporating an electron-acceptor spacer in **L110** or **L113** might help

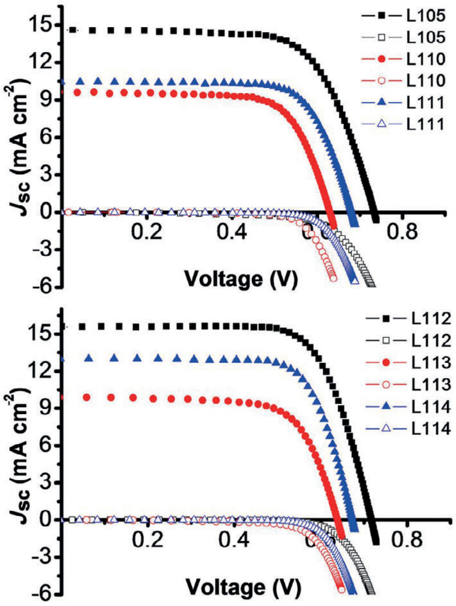

Figure 5. CV spectra of H111 (Δ), H112 (○) and spiro-OMeTAD (solid line).

adjust the electron structure to a more desirable direction; whereas in the case of dyes with a weak donor, such as **L111** and **L114**, an electron-rich π spacer was essential to extend absorption.

Electrochemical impedance spectroscopy

The charge-recombination process is one of the major limiting factors with regard to cell performance. It is related to interfacial processes and determined by the type of sensitizer, the method of deposition, the use of additional coatings, and the type of electrolyte in liquid DSCs.[15] Plots of recombination resistance (R_{rec}) versus the common equivalent conduction-band voltage (V_{ecb}) for the six dyes are shown in Figure 6 by fitting the data obtained from electrochemical impedance spectroscopy (EIS) to a Bisquert equivalent circuit model for liquid DSCs.[16] The applied voltage (*x* axis) was rescaled as a function of V_{ecb}, taking into account the shift in chemical capacitance to eliminate the effect of the TiO_2 conduction-band (CB) position. EIS results showed that **L105** and **L112** had the highest recombination resistance, whereas **L110** and **L113** had the lowest values. This observation was consistent with photovoltaic measurements, according to which **L105** and **L112** had the highest V_{oc} values (~0.73 V), whereas **L110** and **L113** had V_{oc} values that were as low as 0.63 eV with the values of recombination resistance (and V_{oc}) of **L111** and **L114** lying in between. From both EIS and photovoltaic measurements we can conclude that donor units largely determine V_{oc} values, whereas the two different π spacers, playing an important role in modulating absorption, had little effect on recombination rate. For **L110** and **L113**, the higher HOMO levels of **L110** and **L113** limited the charge transfer of photon-excited electrons to the CB of TiO_2, thus leading to a higher chance of recombination. As discussed earlier, the π spacer largely replaced the carbazole moiety as donor in both **L105** and **L114**; the large and rigid carbazole group might impede electron transport from I_3^- to the more embedded oxidized site. On the other hand, it might also mitigate electron loss from TiO_2 surface to I_3^-, leading to a slightly better FF of **L111** and **L114** relative to the rest of the dyes (Table 2).

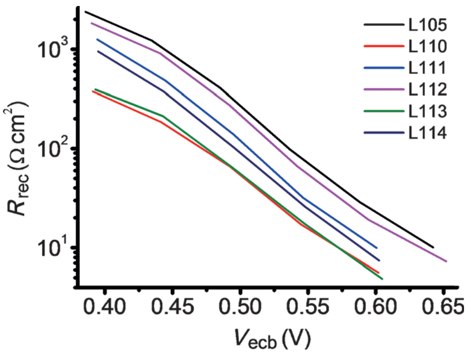

Figure 6. Recombination resistance of DSCs sensitized with the six dyes.

Charge-transfer kinetics

The electron-recombination kinetics were further investigated by studying the photovoltage response of DSCs to a small light-amplitude modulation. For complete solar cells, the electron lifetime as a function of open-circuit potential of DSCs based on the six different dyes was measured, and the measured electron lifetime was plotted as a function of the quasi-Fermi level of TiO_2 (Figure 7). Under conditions of equal internal potential in TiO_2, implying also equal electron concentration in TiO_2 because no band-edge shifts or changes in trap distribution are expected (see below), the electron lifetime for DSCs based on **L105** and **L112** was much longer than that of other dyes (especially for **L110** and **L113**). Electron lifetimes in DSCs usually reflect electron recombination with the oxidized form of the redox species in the electrolyte; in cases of slow regeneration of the oxidized dye, however, the effect of electron recombination to the oxidized dye will also be included in the measured lifetime. Dye regeneration by **L110** and **L113** is rather slow, and significant recombination of electrons in TiO_2 to the oxidized dye may account for the short electron lifetime. The observed trend of increase in recombination is in agreement with the changes of V_{oc} for the different dyes, which further confirm that unsuitable donor structures (**L110** and **L113**) cause more serious recombination problems.

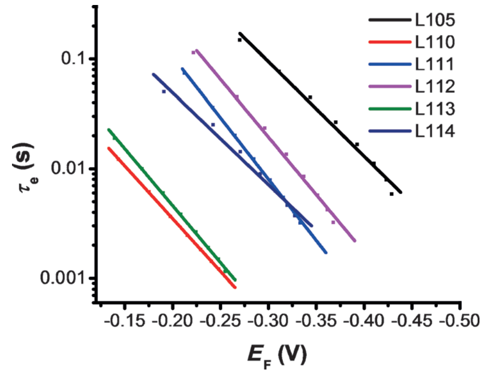

Figure 7. Electron lifetime as a function of the quasi-Fermi level of the TiO_2 under open-circuit conditions for DSCs sensitized with all six dyes employing iodide/triiodide electrolyte.

Photoinduced absorption spectroscopy (PIA) analysis was performed under conditions similar to the operational conditions of DSCs to obtain spectra for the oxidized dye (the oxidized dye absorption spectra were confirmed by spectroelectrochemistry measurements, see below). As seen in Figure 8, the absorption peak appearing at 700–800 nm for **L105** and 700–900 nm for **L112**, should be ascribed to the absorption peaks of oxidized **L105** and **L112**, respectively. After adding iodide/triiodide electrolyte, the peaks of the oxidized dyes disappear rapidly, which indicates an efficient regeneration process on a millisecond timescale. However, for **L110** and **L113**, upon addition of iodide/triiodide electrolyte, the oxidized dye peaks still exhibit strong intensities, which signal inefficient regeneration of these two dyes. These results verified our hy-

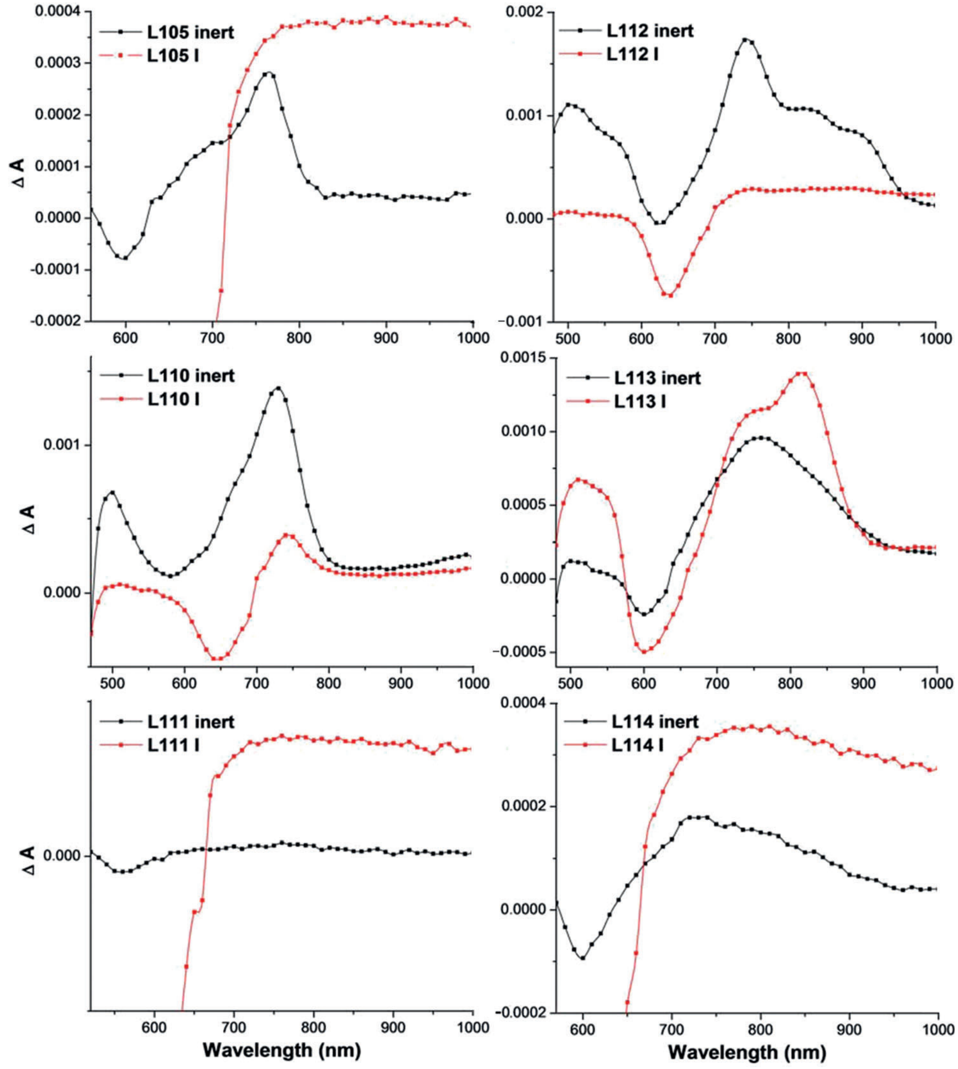

Figure 8. PIA spectra of TiO_2 sensitized with all six different dyes based on inert electrolyte (black) and iodide/triodide electrolyte (red).

pothesis that the apparent lower J_{sc} values for **L110** and **L113** relative to the other four dyes were caused most possibly by decreased regeneration efficiency due to the extremely low HOMO potential level of these two dyes. In other words, the lower driving force for the regeneration of **L110** and **L113** caused serious decreases in current and IPCE values. To confirm the presence of the oxidized dyes, we performed spectroelectrochemistry analyses on dyes attached to mesoporous TiO_2. The spectral changes of the six dyes during oxidation in a solution of $LiClO_4$ in acetonitrile (0.1 M) are shown in the Supporting Information (Figure S5). All six dyes showed strong absorption bands in the longer wavelength region, which was due to the oxidation process, as well as ground-state bleaching bands from 400–600 nm.

Conclusions

We report on six donor–spacer–acceptor organic dyes designed by a permutation of three structurally correlated triarylamine derivatives and two π spacers based on the cyclopenta[1,2-b:5,4-b′]dithiophene (CPDT) and the more extended cyclopenta[1,2-b:5,4-b′]dithiophene[2′,1′:4,5]thieno[2,3-d]thiophene (CPDTTT) structures. For dye molecules **L105**, **L110**, and **L111** (with the CPDT spacer), the different donors had significant effects on their HOMO levels, with **L110** possessing the highest HOMO energy due to its containing the strongest donor. However, such impact was attenuated upon changing the spacer to the more π-extended CPDTTT unit because the more electron-rich CPDTTT itself partially acted as the donor. This helped **L114** to dramatically reduce its bandgap relative to **L111** (with the weakest donor, a carbazole unit). On the other hand, the attempt to reduce the bandgap in order to increase the light-harvesting capability and photovoltaic performance was compromised by the slow dye regeneration because of mismatched energy levels. We thus concluded that when designing a donor–π bridge–acceptor molecule, instead of combining the best electron donors and highest possible π-extending spacers, it is imperative to achieve a good balance between light-harvesting capability and suitable energy level (especially the HOMO level for electron-rich spacers). In this regard it is worth mentioning that we attempted to test a dye molecule (**L108**; see the Supporting Information, Figure S3) by combining compound **8** with 5*H*-[1,2,5]thiadiazolo [3,4-f]isoindole-5,7(6*H*)-dione (a strong electron-accepting spacer).[17] Despite having a broader absorption relative to that of **L101** (data not shown), **L108** displayed poor exciton dissociation accompanied by low J_{sc} and V_{oc} values probably due to the excessively low LUMO energy for electrons to transfer to the conduction band of TiO_2, which is another extreme case of improper energy-band matching in dye design.

Experimental Section

Synthesis

All reactions were carried out under a N_2 atmosphere. Column chromatography was carried out with Merck silica (230–400 mesh), whereas thin-layer chromatography (TLC) was performed on Merck silica 60 Al-backed plates (20 cm×20 cm). Compounds **1**,[17] **2**,[18] **3**,[19] **4**,[13] and **L105**[19] were synthesized according to literature procedures. Compounds **8** and **11** were used after reaction without further purification as it was found they underwent partial decomposition during attempted purification by column chromatography.

***N*,*N*-bis(4-methoxyphenyl)thiophen-2-amine (7):** Compound **6** (2 g, 8.72 mmol), 2-bromothiophene (1.7 g, 10.5 mmol), *t*BuOK (2.95 g, 26.3 mmol), [Pd(dba)$_2$] (0.50 g, 0.87 mmol), and P(*t*Bu)$_3$·HBF$_4$ (0.25 g, 0.87 mmol) were dissolved in dry toluene (20 mL). The solution was heated to 95 °C for 1 d; it was subsequently cooled to room temperature and the solvent was removed under reduced pressure. The residue was extracted with dichloromethane. The extract was washed with water, dried over anhydrous $MgSO_4$, and filtered. The filtrate was evaporated and the residue was purified by flash column chromatography on silica using DCM/hexane = 1:2 (*v*/*v*) as eluent to yield **7** as a light yellow semisolid (2.2 g, 80 %). ^{1}H NMR (400 MHz, $CDCl_3$): δ = 7.06 (d, *J* = 8.8 Hz, 4 H, Ph**H**), 6.79–6.82 (m, 6 H, Ph**H**, Th**H**), 6.55 (br, 1 H, Th**H**), 3.79 ppm (s, 6 H, OC**H$_3$**); ^{13}C NMR (100 MHz, $CDCl_3$): δ = 156.2, 154.1, 142.6, 126.5, 124.8, 118.7, 118.4, 115.1, 56.2 ppm; MS (MALDI-TOF): *m*/*z*: 311.08 (M^+); calcd *m*/*e* (100 %): 311.10; elemental analysis calcd (%) for $C_{18}H_{17}NO_2S$: C, 69.43; H, 5.50; N, 4.50; S, 10.30; found: C, 69.19; H, 5.67; N, 4.68; S, 10.04.

3,6-di-*tert*-butyl-9-(thiophen-2-yl)-9*H*-carbazole (10): Compound **10** was synthesized by the method used for the synthesis of **7**. After being purified by flash column chromatography on silica using DCM/hexane = 1:4 (*v*/*v*) as eluent, a white solid was obtained with a yield of 85 %. ^{1}H NMR (400 MHz, $CDCl_3$): δ = 8.15 (s, 2 H, Ph**H**), 7.52 (dd, *J* = 8.8 Hz, 2 H, Ph**H**), 7.42 (d, *J* = 8.8 Hz, 2 H, Ph**H**), 7.36 (dd, *J* = 5.2 Hz, Th**H**), 7.18 (m, 2 H, Th**H**), 1.50 ppm (s, 18 H, C**H$_3$**); ^{13}C NMR (100 MHz, $CDCl_3$): δ = 144.2, 141.1, 140.1, 126.8, 124.7, 124.6, 124.3, 124.1, 116.9, 110.3, 35.5, 32.7 ppm; MS (MALDI-TOF) *m*/*z*: 361.16 (M^+); calcd *m*/*e* (100 %): 361.19; elemental analysis calcd (%) for $C_{24}H_{27}NS$: C, 79.73; H, 7.53; N, 3.87; S, 8.87; found: C, 79.87; H, 7.39; N, 4.09; S, 8.65.

Aldehyde precursor of L110 (12): Compound **2** (0.4 g, 0.88 mmol), compound **8** (0.8 g, 1.33 mmol), and Pd(PPh$_3$)$_2$Cl$_2$ (50 mg, 0.071 mmol) were added to a round-bottom flask (50 mL) purged with N_2 gas, followed by addition of of freshly distilled THF (20 mL). The reaction mixture was stirred under reflux for 3 h. The mixture was cooled and was then poured into water and extracted with DCM. The organic layer was collected, dried over anhydrous $MgSO_4$, and concentrated. The filtrate was evaporated and the residue was purified by flash column chromatography on silica using DCM/hexane = 3:1 (*v*/*v*) as eluent to yield **12** as a deep red solid (0.41 g, 68 %). ^{1}H NMR (400 MHz, $CDCl_3$): δ = 9.79 (s, 1 H, C**H**O), 7.51 (s, 1 H, Th**H**), 7.14 (d, *J* = 88 Hz, 4 H, Ph**H**), 6.95 (s, 1 H, Th**H**), 6.82–6.86 (m, 6 H, Ph**H**, Th**H**), 3.80 (s, 6 H, OC**H$_3$**), 1.78–1.85 (m, 4 H, C(C**H$_2$**)$_2$), 1.11–1.33 (m, 12 H, C**H$_2$**), 0.90–0.94 (m, 4 H, C**H$_2$**), 0.87 ppm (t, *J* = 7.2 Hz, 6 H, C**H$_3$**); ^{13}C NMR (100 MHz, $CDCl_3$): δ = 182.9, 164.0, 157.9, 157.0, 154.7, 144.0, 143.2, 141.5, 133.4, 131.5, 129.4, 127.8, 125.8, 123.7, 117.0, 116.0, 115.3, 115.2, 56.2, 38.4, 32.2, 30.2, 25.1, 23.2, 14.7 ppm; MS (MALDI-TOF) *m*/*z*: 683.28 (M^+); calcd *m*/*e* (100 %): 683.26; elemental analysis calcd (%) for $C_{40}H_{45}NO_3S_3$: C, 70.24; H, 6.63; N, 2.05; S, 14.06; found: 70.36; H, 6.56; N, 2.19; S, 13.93.

Aldehyde precursor of L111 (14): Compound **14** was synthesized by the method used for the synthesis of **12** by a Stille coupling between compounds **11** and **2**. After being purified by chromatography on silica eluting with DCM/hexane = 3:1 (*v*/*v*), a yellow solid was obtained with a yield of 75 %. ^{1}H NMR (400 MHz, $CDCl_3$): δ = 9.85 (s, 1 H, C**H**O), 8.12 (s, 1 H, Ph**H**), 7.58 (s, 1 H, Th**H**), 7.50–7.52 (m, 4 H, Ph**H**), 7.28 (d, *J* = 4 Hz, 1 H, Ph**H**), 7.11 (d, *J* = 4 Hz, 1 H, Th**H**), 7.09 (s, 1 H, Th**H**), 3.80 (s, 6 H, OC**H$_3$**), 1.87–1.93 (m, 4 H, C(C**H$_2$**)$_2$), 1.48 (s, 18 H, C(C**H$_3$**)$_3$), 1.18–1.22 (m, 12 H, C**H$_2$**), 0.95–0.99 (m, 4 H, C**H$_2$**), 0.84 ppm (t, *J* = 6.8 Hz, 6 H, C**H$_3$**); ^{13}C NMR (100 MHz, $CDCl_3$): δ = 183.2, 163.7, 158.5, 148.1, 144.6, 144.1, 142.4, 140.7, 139.2, 135.7, 135.2, 130.5, 125.4, 124.7, 124.3, 123.2, 118.8, 117.0, 110.3, 54.9, 38.4, 35.4, 32.6, 32.2, 30.3, 27.6, 25.2, 23.3, 14.7 ppm; MS (MALDI-TOF) *m*/*z*: 733.56 (M^+); calcd *m*/*e* (100 %): 733.34; elemental analysis calcd (%) for $C_{46}H_{55}NOS_3$: C, 75.26; H, 7.55; N, 1.91; S, 13.10; found: 75.47; H, 7.45; N, 1.97; S, 13.19.

Aldehyde precursor of L112 (5): Compound **1** (0.11 g, 0.30 mmol), compound **4** (0.3 g, 0.25 mmol), and [Pd(PPh$_3$)$_4$] (20 mg, 0.017 mmol) were added to a round-bottom flask (50 mL) purged with N_2 gas, followed by addition of freshly distilled THF (15 mL) and aq. K_2CO_3 (3 mL, 2 M). The reaction was stirred under reflux for 6 h. The cooled mixture was poured into water and extracted with DCM. The organic layer was collected, dried over anhydrous $MgSO_4$, and concentrated. The filtrate was evaporated and the residue was purified by flash column chromatography on silica using DCM/hexane = 3:1 (*v*/*v*) as eluent to yield **5** as a deep red solid (0.28 g, 80 %). ^{1}H NMR (400 MHz, $CDCl_3$): δ = 9.73 (s, 1 H, C**H**O), 7.62 (s, 1 H, Th**H**), 7.23 (d, *J* = 7.6 Hz, 2 H, Ph**H**), 7.01–7.08 (m, 18 H, Ph**H**, Th**H**), 6.87–6.91 (m, 9 H, Ph**H**, Th**H**), 3.82 (s, 6 H, OC**H$_3$**), 2.58 (t, *J* = 7.6 Hz, 4 H, PhC**H$_2$**), 2.50 (t, *J* = 7.6 Hz, 4 H, PhC**H$_2$**),1.20–1.41 (m, 48 H, C**H$_2$**), 0.86–0.93 ppm (m, 12 H, C**H$_3$**); ^{13}C NMR (100 MHz, $CDCl_3$): δ = 182.6, 173.7, 168.2, 160.4, 157.0, 148.0, 144.2, 143.1, 142.6, 140.9, 140.0, 139.6, 139.2, 133.2, 132.9, 132.8, 132.2, 131.5, 129.4, 129.2, 128.3, 128.2, 127,5, 126.4, 120.4, 118.4, 115.3, 62.8, 56.0, 36.2, 36.1, 32.5, 32.2, 32.0, 30.4, 30.2, 30.1, 30.0, 29.99, 29.94, 23.38, 23.37, 14.6 ppm; MS (MALDI-TOF) *m*/*z*: 1412.70 (M^+); calcd *m*/*e* (100 %): 1412.93; elemental analysis calcd (%) for $C_{93}H_{105}NO_3S_4$: C, 79.05; H, 7.49; N, 0.99; S, 9.08; found: 78.81; H, 7.56; N, 1.04; S, 8.99.

Aldehyde precursor of L113 (13): Compound **13** was synthesized by the method used for the synthesis of **12** through a Stille coupling between **8** and **4** to obtain a deep red solid in 72 % yield. ^{1}H NMR (400 MHz, $CDCl_3$): δ = 9.75 (s, 1 H, C**H**O), 7.64 (s, 1 H, Th**H**), 7.07–7.12 (m, 22 H, Ph**H**, Th**H**), 6.93 (s, 1 H, Th**H**), 6.83 (d, *J* = 8.8 Hz, 4 H, Ph**H**), 3.79 (s, 6 H, OC**H$_3$**), 2.55 (m, 8 H, PhC**H$_2$**), 1.26–1.34 (m, 48 H, C**H$_2$**), 0.87 ppm (t, *J* = 6.8 Hz, 12 H, C**H$_3$**); ^{13}C NMR (100 MHz, $CDCl_3$): δ = 182.9, 159.5, 157.7, 156.8, 153.8, 153.5, 148.6, 148.3, 143.7, 143.0, 142.7, 141.7, 140.8, 139.8, 139.3, 135.8, 135.1, 134.6, 129.4, 129.3, 128.3, 125.5, 122.8, 118.9, 116.7, 115.2, 62.9, 62.8, 56.1, 36.2, 32.5, 31.9, 30.4, 30.1, 29.9, 23.3, 14.8 ppm; MS (MALDI-TOF) *m*/*z*: 1418.68 (M^+); calcd *m*/*e* (99.7 %): 1418.66; elemental analysis calcd (%) for $C_{91}H_{103}NO_3S_5$: C, 77.02; H, 7.32; N, 0.99; S, 11.30; found: 77.29; H, 7.25; N, 0.94; S, 11.18.

Aldehyde precursor of L114 (15): Compound **15** was synthesized by the method used for the synthesis of **14** through a Stille coupling between **11** and **4** to obtain a red brown solid in 78 % yield. ^{1}H NMR (400 MHz, $CDCl_3$): δ = 9.78 (s, 1 H, C**H**O), 8.11 (s, 2 H, Ph**H**), 7.67 (s, 1 H, Th**H**), 7.50 (dd, *J* = 8.4 Hz, 2 H, Ph**H**), 7.45 (d, *J* = 8.8 Hz, 2 H, Ph**H**), 7.06–7.18 (m, 19 H, Ph**H**, Th**H**), 2.55–2.59 (m, 8 H, PhC**H$_2$**), 1.47 (s, 18 H, C(C**H$_3$**)$_3$), 1.27 (br, 48 H, C**H$_2$**), 0.85–0.89 ppm (m, 12 H, C**H$_3$**); ^{13}C NMR (100 MHz, $CDCl_3$): δ = 182.9, 159.4, 157.8, 153.4, 149.0, 148.4, 144.5, 144.0, 143.1, 142.8, 140.7, 140.3, 139.9, 139.7, 139.4, 139.2, 138.8, 138.5, 136.3, 136.1, 135.7, 129.48, 129.43, 128.4, 128.3, 125.4, 124.6, 124.3, 122.4, 120.5, 116.9, 114.7, 110.3, 63.0, 62.8, 36.2, 35.4, 32.68, 32.64, 32.5, 32.0, 30.4, 30.1, 30.0, 29.9, 23.4, 23.3, 14.8 ppm; MS (MALDI-TOF) *m/z*: 1468.68 (M^+); calcd *m/e* (100%): 1468.75; elemental analysis calcd (%) for $C_{97}H_{113}NOS_5$: C, 79.29; H, 7.75; N, 0.95; S, 10.91; found: C, 79.55; H, 7.68; N, 0.98; S, 10.73.

L110: Compound **12** (0.2 g, 0.29 mmol), cyanoacetic acid (74 mg, 0.87 mmol), and piperidine (150 mg, 1.74 mmol) were added to a round-bottom flask (50 mL) purged with N_2 gas, followed by addition of dry chloroform (15 mL). The solution was heated to reflux overnight, cooled, acidified with HCl (1 M), poured into water, and then extracted with DCM. The organic layer was collected, washed with water, and concentrated. The residue was purified by flash column chromatography using DCM/MeOH = 9:1 (*v/v*) as eluent to obtain a black solid (152 mg, 70%). ^{1}H NMR (400 MHz, CD_2Cl_2): δ = 8.36 (s, 1H, Th**H**), 7.60 (s, 1H, Th**H**), 7.13–7.15 (br, 5H, Ph**H**, Th**H**), 6.85–6.87 (br, 6H, Ph**H**, Th**H**, vinyl **H**), 6.28 (br, 1H, Th**H**), 3.80 (s, 6H, OC**H$_3$**), 1.85 (br, 4H, C(C**H$_2$**)$_2$) 1.14 (br, 12H, C**H$_2$**), 0.91–0.96 (br, 4H, C**H$_2$**), 0.80–0.82 ppm (m, 6H, C**H$_3$**); ^{13}C NMR (100 MHz, CD_2Cl_2): δ = 165.0, 158.6, 156.8, 151.7, 151.5, 149.3, 149.2, 148.9, 147.8, 146.5, 140.7, 138.4, 136.5, 134.0, 129.4, 128.6, 127.3, 126.6, 120.3, 116.8, 115.1, 68.2, 55.9, 38.0, 32.0, 30.0, 26.0, 25.0, 23.0, 14.2 ppm; MS (MALDI-TOF) *m/z*: 750.55; calcd *m/e* (100%): 750.27; elemental analysis calcd (%) for $C_{43}H_{46}N_2O_4S_3$: C, 68.77; H, 6.17; N, 3.73; S, 12.81; found: C, 69.10; H, 6.05; N, 3.61; S, 12.67.

L111: Dye **L111** was synthesized from **14** by the method used for the synthesis of **L110** to obtain a red solid in 82% yield. ^{1}H NMR (400 MHz, CD_2Cl_2): δ = 8.47 (s, 1H, Th**H**), 8.12 (br, 2H, Ph**H**), 8.06 (s, 1H, Th**H**), 7.72 (s, 1H, Th**H**), 7.42 (br, 3H, Th**H**, Ph**H**), 7.17–7.23 (m, br, 2H, Ph**H**), 7.05 (br, 1H, vinyl **H**), 1.95 (br, 4H, C(C**H$_2$**)$_2$), 1.44 (s, 18H, C(C**H$_3$**)$_3$), 1.21 (br, 12H, C**H$_2$**), 1.08 (br, 4H, C**H$_2$**), 0.84 ppm (t, *J* = 6.4 Hz, 6H, C**H$_3$**); ^{13}C NMR (100 MHz, CD_2Cl_2): δ = 163.9, 163.5, 159.2, 148.6, 147.4, 144.4, 142.6, 140.3, 138.9, 137.5, 135.3, 135.2, 131.5, 128.6, 125.0, 124.4, 124.0, 122.9, 118.8, 116.7, 115.0, 110.0, 68.2, 38.0, 37.0, 35.0, 32.1, 30.1, 25.1, 23.1, 14.3 ppm; MS (MALDI-TOF) *m/z*: 800.74; calcd *m/e* (100%): 800.35; elemental analysis calcd (%) for $C_{49}H_{56}N_2O_2S_3$: C, 73.46; H, 7.05; N, 3.50; S, 12.01; found: C, 73.69; H, 7.02; N, 3.28; S, 12.17.

L112: Dye **L112** was synthesized from **5** by the method used for the synthesis of **L110** to obtain a dark purple solid in 75% yield. ^{1}H NMR (400 MHz, CD_2Cl_2): δ = 8.19 (br, 1H, Th**H**), 7.42 (d, *J* = 8.4 Hz, 2H, Ph**H**), 7.21 (s, 1H, Th**H**), 7.07–7.16 (m, br, 15H, Ph**H**, Th**H**), 6.98 (br, 4H, Ph**H**), 6.86–6.90 (m, br, 8H, Ph**H**, Th**H**, vinyl **H**), 3.82 (s, 6H, OC**H$_3$**), 2.45 to 2.55 (br, 8H, C(C**H$_2$**)$_2$), 1.17–1.45 (m, br, 48H, C**H$_2$**), 0.83 ppm (t, *J* = 6.8 Hz, 12H, C**H$_3$**); ^{13}C NMR (100 MHz, CD_2Cl_2): δ = 163.4, 159.7, 157.5, 156.7, 152.9, 148.9, 148.1, 147.3, 142.7, 142.6, 140.8, 139.7, 139.0, 137.4, 136.0, 135.0, 134.8, 132.9, 129.1, 128.1, 127.2, 126.9, 126.3, 120.5, 118.1, 115.1, 62.9, 62.5, 55.9, 35.9, 32.3, 31.9, 31.7, 29.94, 29.92, 29.8, 29.7, 23.1, 14.36, 14.35 ppm; MS (MALDI-TOF) *m/z*: 1479.71; calcd *m/e* (100%): 1479.56; elemental analysis calcd (%) for $C_{96}H_{106}N_2O_4S_4$: C, 77.90; H, 7.22; N, 1.89; S, 8.67; found: C, 77.82; H, 7.29; N, 1.86; S, 8.55.

L113: Dye **L113** was synthesized from **13** by the method used for the synthesis of **L110** to obtain a black solid in 67% yield. ^{1}H NMR (400 MHz, CD_2Cl_2): δ = 8.17 (s, 1H, ThH), 6.86–7.15 (m, br, 28H, Th**H**, Ph**H**, vinyl **H**), 6.36 (br, 1H, ThH), 3.82 (s, 6H, OC**H$_3$**), 2.38–2.56 (br, 8H, C(C**H$_2$**)$_2$), 1.15–1.43 (m, br, 48H, C**H$_2$**), 0.82–0.86 ppm (m, 12H, C**H$_3$**); ^{13}C NMR (100 MHz, CD_2Cl_2): δ = 165.1, 159.3, 158.8, 158.4, 157.5, 156.8, 153.8, 148.2, 146.2, 142.7, 142.6, 141.4, 140.6, 140.2, 139.5, 139.0, 138.7, 136.2, 136.1, 135.1, 135.1, 134.4, 129.8, 129.3, 129.1, 128.1, 127.8, 125.4, 122.6, 118.5, 116.1, 115.3, 115.0, 114.5, 63.0, 62.8, 62.5, 55.9, 36.0, 32.35, 32.33, 31.9, 31.7, 29.9, 29.8, 29.7, 23.1, 14.3 ppm; MS (MALDI-TOF) *m/z*: 1485.55; calcd *m/e* (100%): 1485.66; elemental analysis calcd (%) for $C_{94}H_{104}N_2O_4S_5$: C, 75.97; H, 7.05; N, 1.88; S, 10.79; found: C, 75.74; H, 7.19; N, 1.93; S, 10.66.

L114: Dye **L114** was synthesized from **15** by the method used for the synthesis of **L110** to obtain a black solid in 75% yield. ^{1}H NMR (400 MHz, CD_2Cl_2): δ = 8.16 (m, br, 3H, Th**H**, Ph**H**), 7.48–7.56 (m, 4H, PhH), 7.26–7.28 (m, 2H, Ph**H**), 7.02–7.18 (m, br, 19H, Th**H**, Ph**H**, vinyl **H**), 2.49–2.58 (br, 8H, C(C**H$_2$**)$_2$), 1.49 (s, 18H, C(C**H$_3$**)$_3$), 1.20–1.39 (m, br, 48H, C**H$_2$**), 0.84–0.86 ppm (br, 12H, C**H$_3$**); ^{13}C NMR (100 MHz, CD_2Cl_2): δ = 159.4, 157.8, 153.1, 150.5, 148.9, 146.8, 144.4, 142.9, 142.8, 140.5, 140.1, 139.7, 139.4, 138.9, 138.3, 137.5, 136.5, 136.2, 135.7, 135.6, 129.2, 128.1, 125.2, 124.4, 124.0, 122.4, 120.3, 116.7, 110.0, 109.4, 63.0, 62.6, 36.0, 35.1, 32.3, 32.1, 31.9, 31.8, 29.93, 29.90, 29.7, 23.1, 14.38, 14.36 ppm; MS (MALDI-TOF) *m/z*: 1535.75; calcd *m/e* (100%): 1535.78; elemental analysis calcd (%) for $C_{100}H_{114}N_2O_2S_5$: C, 78.18; H, 7.48; N, 1.82; S, 10.44; found: C, 77.90; H, 7.57; N, 1.89; S, 10.40.

Device fabrication

A fluorine-doped tin oxide (FTO) glass plate was immersed in a solution of Decon soap and was decontaminated under ultrasonic irradiation for 30 min; it was then transferred to aq. $TiCl_4$ (0.04 M), was heated at 70 °C for 30 min, and washed with deionized water and ethanol. Nanocrystalline TiO_2 paste was coated on top of the FTO glass by the manual screen-printing method (4×4 mm active area for each cell). Two transmission layers (particle size of 18 nm) and two reflection layers (particle size of 150 nm) were printed in sequence with a relaxation time of 6 min and annealed at 125 °C for each layer. The 2+2 TiO_2-coated FTO glass was sintered at 500 °C, was then post-treated in aq. $TiCl_4$ (0.04 M) at 70 °C for 30 min, and washed with deionized water and ethanol. The prepared TiO_2 electrodes were immersed into dye solutions (0.2 mM) and kept at room temperature for 6 h. Counter electrodes were prepared by drilling a hole on the cleaned FTO glass followed by coating a drop of a solution of H_2PtCl_6 in isopropyl alcohol (8 mM) and heating at 400 °C for 15 min. The dye-adsorbed TiO_2 electrode and Pt counter electrode were assembled and sealed with a Surlyn film (25 μm in thickness) under a hot-press. The cell was filled with a drop of the electrolyte (Z960) comprising 1,3-dimethylimidazolium iodide (DMII, 1.0 M), LiI (0.05 M), I_2 (0.03 M), 4-*tert*-butylpyridine (TBP, 0.5 M), guanidiniumthiocyanate (GuSCN, 0.1 M) in acetonitrile/valeronitrile = 85:15 (*v/v*) by means of vacuum backfilling. The hole was quickly sealed with a Surlyn film covered with glass. Finally, the contacts were soldered with Sn metal at 280 °C and 60 kHz.

Equipment

^{1}H and ^{13}C NMR data were obtained on a Bruker DPX (400 and 100 MHz, respectively) spectrometer with chemical shifts referenced to $CDCl_3$ or CD_2Cl_2. Matrix-assisted laser desorption/ionization time-of-flight (MALDI-TOF) mass spectra were obtained on a Shimadzu Biotech AXIMA-TOF^2. Elemental analysis was obtained using a Thermo Scientific Flash 2000 Series CHNS/O Analyzer. UV/Vis absorption spectra in solution were recorded using a UV-3600 spectrophotometer. The absorption of the dye-loaded photoanode was measured with an integrating sphere attachment (ISR-3100) loaded onto the UV/Vis-NIR spectrophotometer. The interior of the integrating sphere was coated with $BaSO_4$ with an incident angle of 8° for total reflectance measurement. Although transmittance and reflectance could be measured directly by photospectroscopy, absorption was calculated using the law of energy conversion (Absorbance% = 100% − Transmittance% − Reflectance%). CV experiments were performed using a Multichannel Potentiostat (Model 1470E) from Solartron Analytical. All CV measurements were recorded in DCM with tetrabutylammonium hexafluorophosphate (0.1 M) as supporting electrolyte (scan rate of 100 mV s^{-1}). The experiments were performed at room temperature with a conventional three-electrode configuration consisting of a platinum wire working electrode, a gold counter electrode, and an Ag/AgCl in aq. KCl (3 M) reference electrode. The measured potentials were converted to orbital energies by calibration using the ferrocene/ferrocenium (Fc/Fc$^+$) redox couple. For photovoltaic measurements, solar cells with an active area of 0.16 cm^{-2} were measured through a metal mask (0.25 cm^{-2}) using a solar simulator (San-EI Electric, XEC-301S) under AM 1.5G irradiation. *J–V* characteristics were recorded by applying an external potential bias while measuring the current response using a Keithley 2612 A SourceMeter. EIS analyses were carried out using the AutoLab PGSTAT302N under illumination condition with different bias potentials being applied, ranging from 0.05 V to open-circuit voltage and frequencies between 1 MHz and 1 Hz. IPCE studies were carried out using PVE300 from Bentham, with a dual Xenon/quartz halogen light source, measured in DC mode.

Photoinduced absorption spectroscopy (PIA) measurements were performed on a similar setup as that described in the literature.[20] Samples were prepared by the method described above except that two different electrolytes were used: an inert electrolyte consisting of TBP (0.5 M) and GuSCN (0.1 M) in acetonitrile/valeronitrile = 85:15 (*v*/*v*) and an iodide/triiodide electrolyte (Z960). A square-wave modulated blue light-emitting diode (LED, Luxeon Star 1 W, Royal Blue, 460 nm) used for excitation was superimposed on a white probe light provided by a tungsten–halogen lamp (20 W). The transmitted probe light was focused onto a monochromator (Acton Research Corp. SP-150) and detected using a UV-enhanced Si photodiode, connected to a lock-in amplifier (Stanford Research Systems model SR830) by a current amplifier (Stanford Research Systems model SR570). The intensity of the probe light was approximately 100 W m^{-2}, and the intensity of the excitation LED was approximately 80 W m^{-2}. The modulation frequency of the LED was 9.33 Hz. ΔA was calculated from the in-phase and out-of-phase parts of the change in transmission.

Electron lifetime and extracted charge measurements were performed using a white LED (Luxeon Star 1 W) as the light source. Voltage traces were recorded with a 16-bit resolution digital acquisition board (National Instruments) in combination with a current amplifier (Stanford Research Systems SR570) and a custom-made system using electromagnetic switches. Lifetimes were determined by monitoring photovoltage transients at different light intensities upon applying a small square-wave modulation to the base light intensity. The photovoltaic responses were fitted using first-order kinetics to obtain time constants.[21] Extracted charge measurements were performed by illuminating the cell for 5 s under open-circuit conditions and then turning the lamp off to let the voltage decay to a voltage *V*. The cell was then short circuited, and the current was measured for 5 s and integrated to obtain Q_{oc} (V).

Spectroelectrochemistry was performed on a potentiostat with a three-electrode setup (CH Instruments 660). At the same time as performing the electrical measurements, UV/Vis spectra were recorded. All six different dye-coated mesoporous TiO_2 films were used as working electrodes. A glassy-carbon electrode was used as the counter electrode and a Ag/Ag$^+$ electrode as a pseudo reference electrode. The electrolyte solution was $LiClO_4$ (0.1 M) in acetonitrile. The system was internally calibrated with the ferrocene/ferrocenium (Fc/Fc$^+$) redox couple using a platinum working electrode. CV analyses of TiO_2 films were performed in the $LiClO_4$ supporting electrolyte with a scan rate of 50 mV s^{-1}. Data analyses were performed in MATLAB.

Acknowledgements

We acknowledge funding from the National Research Foundation Singapore through CRP Award NRF-CRP4–2008–03. We thank Professor Subodh Mhaisalkar of ERI@N for his support, encouragement and helpful comments and suggestions.

Keywords: cyclic voltammetry · density functional calculations · dyes/pigments · electrochemistry · solar cells

[1] B. O'Regan, M. Grätzel, *Nature* **1991**, *353*, 737–740.

[2] a) A. Hagfeldt, G. Boschloo, L. Sun, L. Kloo, H. Pettersson, *Chem. Rev.* **2010**, *110*, 6595–6663; b) L.-L. Li, E. W.-G. Diau, *Chem. Soc. Rev.* **2013**, *42*, 291–304; c) M. Grätzel, *Inorg. Chem.* **2005**, *44*, 6841–6851.

[3] a) M. Liang, J. Chen, *Chem. Soc. Rev.* **2013**, *42*, 3453–3488; b) R. K. Kanaparthi, J. Kandhadi, L. Giribabu, *Tetrahedron* **2012**, *68*, 8383–8393.

[4] a) L. Etgar, T. Moehl, S. Gabriel, S. G. Hickey, A. Eychmüller, M. Grätzel, *ACS Nano* **2012**, *6*, 3092–3099; b) K. Yan, L. Zhang, J. Qiu, Y. Qiu, Z. Zhu, J. Wang, S. Yang, *J. Am. Chem. Soc.* **2013**, *135*, 9531–9539; c) C. Yuan, G. Chen, P. N. Prasad, T. Y. Ohulchanskyy, Z. Ning, H. Tian, L. Sun, H. Agren, *J. Mater. Chem.* **2012**, *22*, 16709–16713; d) L. Mu, C. Liu, J. Jia, X. Zhou, Y. Lin, *J. Mater. Chem. A* **2013**, *1*, 8353–8357; e) P. Sheng, W. Li, J. Cai, X. Wang, X. Tong, Q. Cai, C. A. Grimes, *J. Mater. Chem. A* **2013**, *1*, 7806–7815; f) G. Hodes, D. Cahen, *Acc. Chem. Res.* **2012**, *45*, 705–713.

[5] a) J.-Y. Jeng, Y.-F. Chiang, M.-H. Lee, S.-R. Peng, T.-F. Guo, P. Chen, T.-C. Wen, *Adv. Mater.* **2013**, *25*, 3727–3732; b) B. Cai, Y. Xing, Z. Yang, W.-H. Zhang, J. Qiu, *Energy Environ. Sci.* **2013**, *6*, 1480–1485; c) L. Etgar, P. Gao, Z. Xue, Q. Peng, A. K. Chandiran, B. Liu, M. K. Nazeeruddin, M. Grätzel, *J. Am. Chem. Soc.* **2012**, *134*, 17396–17399; d) J. H. Noh, N. J. Jeon, Y. C. Choi, M. K. Nazeeruddin, M. Grätzel, S. I. Seok, *J. Mater. Chem. A* **2013**, *1*, 11842–11847; e) J.-H. Im, C.-R. Lee, J.-W. Lee, S.-W. Park, N.-G. Park, *Nanoscale* **2011**, *3*, 4088–4093; f) I. E. Rauda, R. Senter, S. H. Tolbert, *J. Mater. Chem. C* **2013**, *1*, 1423–1427; g) J. H. Heo, S. H. Im, J. H. Noh, T. N. Mandal, C.-S. Lim, J. A. Chang, Y. H. Lee, H.-j. Kim, A. Sarkar, M. K. Nazeeruddin, M. Grätzel, S. I. Seok, *Nat. Photonics* **2013**, *7*, 486–491; h) M. Liu, M. B. Johnston, H. J. Snaith, *Nature* **2013**, *501*, 395–398; i) H.-S. Kim, C.-R. Lee, J.-H. Im, K.-B. Lee, T. Moehl, A. Marchioro, S.-J. Moon, R. Humphry-Baker, J.-H. Yum, J. E. Moser, M. Grätzel, N.-G. Park, *Sci. Rep.* **2012**, *2*, 591; j) M. M. Lee, J. Teuscher, T. Miyasaka, T. N. Murakami, H. J. Snaith, *Science* **2012**, *338*, 643–647.

[6] A. Yella, H.-W. Lee, H. N. Tsao, C. Yi, A. K. Chandiran, M. K. Nazeeruddin, E. W.-G. Diau, C.-Y. Yeh, S. M. Zakeeruddin, M. Grätzel, *Science* **2011**, *334*, 629–634.

[7] S. Mathew, A. Yella, P. Gao, R. Humphry-Baker, F. E. CurchodBasile, N. Ashari-Astani, I. Tavernelli, U. Rothlisberger, M. K. Nazeeruddin, M. Grätzel, *Nat. Chem.* **2014**, *6*, 242–247.

[8] Z. Ning, Y. Fu, H. Tian, *Energy Environ. Sci.* **2010**, *3*, 1170–1181.

[9] T. Marinado, K. Nonomura, J. Nissfolk, M. K. Karlsson, D. P. Hagberg, L. Sun, S. Mori, A. Hagfeldt, *Langmuir* **2010**, *26*, 2592–2598.

[10] H. N. Tsao, C. Yi, T. Moehl, J.-H. Yum, S. M. Zakeeruddin, M. K. Nazeeruddin, M. Grätzel, *ChemSusChem* **2011**, *4*, 591–594.

[11] a) R. Li, J. Liu, N. Cai, M. Zhang, P. Wang, *J. Phys. Chem. B* **2010**, *114*, 4461–4464; b) D. Zhou, Q. Yu, N. Cai, Y. Bai, Y. Wang, P. Wang, *Energy Environ. Sci.* **2011**, *4*, 2030–2034.

[12] A. Yella, R. Humphry-Baker, B. F. E. Curchod, N. Ashari Astani, J. Teuscher, L. E. Polander, S. Mathew, J.-E. Moser, I. Tavernelli, U. Rothlisberger, M. Grätzel, M. K. Nazeeruddin, J. Frey, *Chem. Mater.* **2013**, *25*, 2733–2739.

[13] H. Bronstein, R. S. Ashraf, Y. Kim, A. J. P. White, T. Anthopoulos, K. Song, D. James, W. Zhang, I. McCulloch, *Macromol. Rapid Commun.* **2011**, *32*, 1664–1668.

[14] N. Cai, R. Li, Y. Wang, M. Zhang, P. Wang, *Energy Environ. Sci.* **2013**, *6*, 139–147.

[15] P. P. Boix, G. Larramona, A. Jacob, B. Delatouche, I. Mora-Seró, J. Bisquert, *J. Phys. Chem. C* **2012**, *116*, 1579 – 1587.

[16] a) F. Fabregat-Santiago, J. Bisquert, E. Palomares, L. Otero, D. Kuang, S. M. Zakeeruddin, M. Grätzel, *J. Phys. Chem. C* **2007**, *111*, 6550 – 6560; b) J. Bisquert, G. Garcia-Belmonte, F. Fabregat-Santiago, N. S. Ferriols, P. Bogdanoff, E. C. Pereira, *J. Phys. Chem. B* **2000**, *104*, 2287 – 2298.

[17] H. Li, T. M. Koh, A. Hagfeldt, M. Grätzel, S. G. Mhaisalkar, A. C. Grimsdale, *Chem. Commun.* **2013**, *49*, 2409 – 2411.

[18] D.-Y. Chen, Y.-Y. Hsu, H.-C. Hsu, B.-S. Chen, Y.-T. Lee, H. Fu, M.-W. Chung, S.-H. Liu, H.-C. Chen, Y. Chi, P.-T. Chou, *Chem. Commun.* **2010**, *46*, 5256 – 5258.

[19] Y. Cao, N. Cai, Y. Wang, R. Li, Y. Yuan, P. Wang, *Phys. Chem. Chem. Phys.* **2012**, *14*, 8282 – 8286.

[20] G. Boschloo, A. Hagfeldt, *Inorg. Chim. Acta* **2008**, *361*, 729 – 734.

[21] G. Boschloo, L. Häggman, A. Hagfeldt, *J. Phys. Chem. B* **2006**, *110*, 13144 – 13150.

Received: July 10, 2014